Cross sections for $A = 6$–30 fragments from the ^{4}He + ^{28}Si reaction at 117 and 198 MeV

L. W. Woo,* K. Kwiatkowski, W. G. Wilson,† and V. E. Viola
Department of Chemistry and IUCF, Indiana University, Bloomington, Indiana 47405

H. Breuer
Department of Physics, University of Maryland, College Park, Maryland 20742

G. J. Mathews
Lawrence Livermore National Laboratory, Livermore, California 94550
(Received 4 August 1992)

Mass, energy, and angular distributions have been measured for $A = 6$–30 fragments formed in the ^{4}He + ^{28}Si reaction at bombarding energies of 117.4 and 198.5 MeV. The data are compared with calculations which account for the reaction dynamics in terms of an intranuclear cascade, followed by statistical decay of the excited residues. General agreement between the data and calculations is found for the spectral shapes and mass distributions; however, the experimental angular distributions are significantly more forward peaked than predicted. This suggests a failure of the model to account satisfactorily for momentum transfer in the collision stage. These results extend linear momentum systematics for ^{4}He projectiles near the Fermi velocity to significantly lower target mass than previously measured. Implications of the data to questions of cosmic ray astrophysics and radiation damage in microelectronic circuits are also discussed.

PACS number(s): 25.55.−e, 98.80.Ft

I. INTRODUCTION

As the relative energy of nucleus-nucleus collisions increases well beyond the interaction barrier, the nuclear reaction mechanisms which contribute to the total reaction cross section become increasingly complex [1]. Above projectile energies of about 10 MeV/nucleon, mean-field processes such as complete fusion and simple two-body transfer reactions gradually diminish in importance while the probability for projectile fragmentation [2, 3], and precompound emission of nucleons [4, 5] and heavier fragments, grows rapidly [6]. This transition is generally understood in terms of the enhanced contribution of nucleon-nucleon scattering to the energy dissipation mechanism as the projectile velocity approaches the Fermi velocity of nucleons in nuclear matter. Because of the continuum/multibody nature of such processes, a full understanding of the reaction dynamics associated with intermediate-energy collisions poses a significant experimental and theoretical challenge.

A parallel goal in the study of nuclear reactions at intermediate energies is to describe the properties and decay characteristics of highly excited nuclear matter. In particular, there is great current interest in the multifragmentation and total disassembly of nuclei at high temperatures [7–11]. Characterization of such events is, however, complicated by the broad spectrum of final states formed in the collision stage. While in principle the full description of such events demands measurements with 4π geometry, valuable insight can be gained from inclusive mass, energy, and angular distributions for the total reaction cross section and comparison of these data with nuclear models.

Previously, doubly differential cross section measurements for all $A \geq 6$ isobars formed in the ^{4}He + ^{12}C reaction [12] have been performed at projectile energies between 50–160 MeV. These data were found to be consistent with an intranuclear cascade/Fermi breakup production mechanism which at the highest energies required significant contributions from three- and four-body breakup events in the decay channel [13]. Total mass yields from the 180-MeV p + ^{27}Al system have also been studied [14]. While the mass yields for this reaction could be accounted for relatively well with a precompound decay reaction mechanism [4] followed by statistical decay of the excited residues, similar comparisons with an intranuclear cascade/statistical decay calculation demonstrated much poorer agreement for both the mass yields and angular distributions. In particular, the standard version of the intranuclear cascade model failed to account for the strong forward-angle peaking of the angular distributions and overpredicted the yields of near-target residues formed in quasifree scattering processes [14]. At the same time the cascade model underpredicted the yields of lighter products formed in higher deposition-energy events. With calculations available at that time, angular distributions could not be calculated

*Present address: Sabbagh Associates, Inc., Bloomington, IN 47408.

†Present address: Kirtland Air Force Base, Albuquerque, NM.

for the precompound decay model and the Fermi breakup code was restricted to nuclei with $A \leq 20$.

In the present work we report inclusive data for mass, kinetic energy and angular distributions from the ^{4}He + ^{28}Si reaction at 117.4 and 198.5 MeV, or $E/A = 29$ and 50 MeV/nucleon. Maximum excitation energies of ~110 and ~180 MeV are possible in these reactions, corresponding to temperatures of 5.2 and 6.7 MeV (assuming $a = A/8$ MeV^{-1}), respectively. The total binding energy for the composite system is 272 MeV. These data provide complete doubly differential cross sections for all isobars with $A = 6$–30 which can then be compared with model predictions. In addition, total reaction cross section estimates and average linear momentum transfer values are obtained [7, 15]. The results are compared with predictions of an intranuclear cascade code, followed by statistical decay of the residual products. The data are also relevant to both astrophysical and radiation damage problems associated with galactic-cosmic ray interactions [16–18].

II. EXPERIMENTAL PROCEDURES

The measurements were performed in the 162-cm-diameter scattering chamber at the Indiana University Cyclotron Facility. Beams of 117.4- and 198.5-MeV ^{4}He ions with intensities 20–100 nA were focused to a 2-mm-diameter spot on a self-supporting, monoisotopic ^{28}Si target of thickness 100 μg/cm^2. Doubly differential cross sections for all isobars with $A = 6$–30 were measured with a five-element time-of-flight detector telescope.

The timing start detector in the telescope consisted of a channel-plate fast-timing detector system which employed 18-mm diameter active-area channel plates [19, 20]. This device was placed 18.4 cm from the ^{28}Si target. Time-of-flight stop signals were derived from a 47-μm thick, 100 mm^2 active area surface-barrier transmission detector placed 48.8 cm from the channel plate device. This system provided a timing resolution of less than 150 psec, yielding a mass resolution of 0.7 u FWHM at 5 MeV for $A = 24$. Relative linearity was verified with timing calibrations performed with a time calibrator. Channel plate efficiencies were checked using particle-identified fragments detected in the silicon $\Delta E - E$ elements of the telescope and were found to range from a minimum of 75% for energetic Li ions to nearly 100% for boron ions [12]. Several antiscattering slits were placed between the start and stop detectors. The collimator on the 47-μm detector defined the solid angle of the telescope, which was 0.173 msr, or $\Delta\theta = 0.86°$.

The 47-μm detector served to define the energy E of all fragments which stopped in this element and the energy-loss ΔE of all energetic fragments which punched through it. The third and fourth elements consisted of 500-μm and 2-mm thick surface-barrier detectors which permitted Z and A identification of energetic ions with $Z \leq 4$ produced in these reactions. The final element was a 5-mm lithium-drifted silicon detector which served to veto light ions passing through the stack. Detector energy calibration was performed with ^{148}Gd and ^{241}Am alpha-particle sources and a precision pulse generator. Absolute energy calibrations of the fragment spectra included Z-dependent corrections for energy loss in the target and the channel-plate carbon foil (20 μg/cm^2), as well as detector dead layers. Total system performance permitted identification of all fragments from $A = 6$–30 with energies $E/A \geq 0.1$ MeV. This is an important consideration in the measurement of these reaction products, due to the resultant low-energy components of the energy spectra (see Fig. 1).

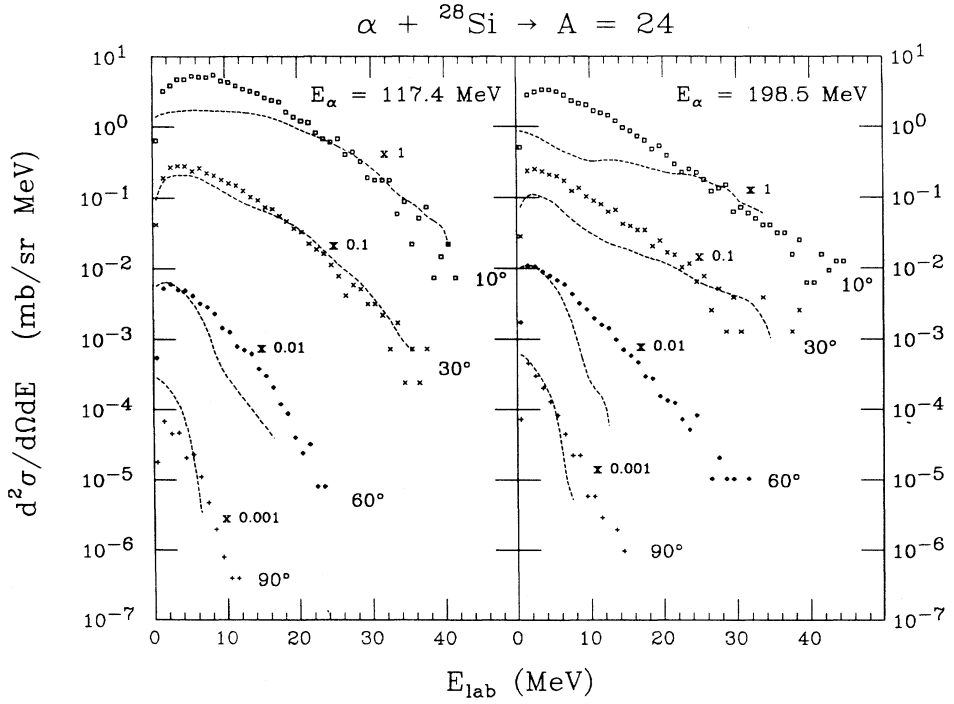

FIG. 1. Energy spectra for $A = 24$ fragments emitted in 117.4 MeV (left) and 198.5 MeV (right) ^{4}He-ion reactions with ^{28}Si. Emission angle is indicated on figure. Dashed lines are the predictions of intranuclear cascade/statistical decay calculations [30].

Linear and logic signals were processed with standard NIM and CAMAC electronics, monitored on-line and stored on magnetic tape for later analysis. Replay was performed on the IUCF VAX system, using the data analysis code LISA [21]. All cross sections were corrected for events which were eliminated by the low-energy threshold of the detection system and for those angles outside the measured range. The low-energy extrapolations were based on the systematic behavior of the data; one-half of the extrapolated counts were added in quadrature to the statistical errors in determining the quoted errors for these measurements. Energy spectra, angular distributions, isobaric cross sections, and linear momentum transfer were determined and catalogued for individual isobars from $A = 6$ to 30. Representative data and isobaric cross section data are presented here; more detailed information is available on request.

III. EXPERIMENTAL RESULTS

The systematic properties of the data obtained in these studies are examined in this section. Energy spectra for $A = 24$ fragments (the dominant isobaric reaction product, see Table I) are shown in Fig. 1 as a function of laboratory angle for both bombarding energies. The Maxwellian shapes for $A = 24$ are representative of all isobaric yields, except for products near the target mass ($A \sim 28$) at angles in the vicinity of the quasielastic recoil angle near 60°. The spectral slopes become increasingly steep as a function of increasing angle, as has been observed previously for the ^{4}He + ^{12}C system [12]. Comparison of the results at the two energies indicates little difference between the spectra, except that at 117.4 MeV the spectral shapes at high fragment energies exhibit a steeper exponential cross section decrease with increasing energy than at 198.5 MeV. Figure 2 shows spectra taken at 30 deg for a range of isobars. This figure demonstrates the relative insensitivity of the spectra to fragment mass. Except for the differences in shape noted above, little dependence on bombarding energy is apparent. Examination of the low-energy maxima in the $A \approx 12$–20 spectra reveals that these peaks are significantly lower than expected for simple Coulomb repulsion associated with a binary breakup processes. The calculated Coulomb peaks for the binary decay channels ^{16}O-^{16}O and ^{12}C-^{20}Ne are indicated by arrows in Fig. 2. This result supports an interpretation in which the light fragments produced in these collisions originate from multibody ($n \geq 3$) final states in the decay channel rather than binary breakup. This implies a broad spectrum of excited states contribute to the final yields, consistent with the expected importance of precompound emission in the collision stage. The results are also in agreement with the observed trends in linear momentum transfer as a function of bombarding energy in this regime of projectile E/A [1, 22].

Angular distributions for a range of isobars are plotted in Fig. 3. All angular distributions are observed to be strongly forward peaked, from which it can be inferred that a significant fraction of the cross section for $A \geq 6$ products is associated with large linear momentum deposition rather than peripheral inelastic processes. Only for $A = 28$ is there a significant deviation from the exponential decrease of the differential cross sections with angle; this occurs in the region near 60°, where quasielastic yields are focused. At both energies the angular distributions become increasingly isotropic as the observed fragment mass decreases. For a given fragment mass the angular distributions exhibit greater isotropy at the higher energy. For example, the forward-to-backward ratios $[F/B = \sigma(15°)/\sigma(165)°]$ for $A = 24$ fragments are $F/B \simeq 20$ at 117.4 MeV and $F/B \simeq 12$ at 198.4 MeV; for $A = 7$ these values are $\simeq 4$ at 117.4 MeV and 3 at 198.5 MeV.

The increasing isotropy of the angular distributions with decreasing fragment mass suggests that large deposition-energy events are accompanied by substantial tranverse momentum components in the entrance and/or exit channels. This may be accounted for in several ways: (1) precompound emission of relatively low energy light particles serves to spread out the angular distribution of primary heavy residues; (2) sequential statistical nucleon and alpha-particle decay may lead to further angular spreading, and (3) instantaneous fragmentation processes – binary or higher order – may produce significant

TABLE I. Total isobaric cross sections (mb).

A	117.4 MeV	198.5 MeV	A	117.4 MeV	198.5 MeV
6	12	13	19	11	17
7	11	15	20	27	30
8	1.2	1.7	21	30	34
9	2.3	3.3	22	37	42
10	4.8	8.0	23	53	57
11	7.5	14	24	80	66
12	18	25	25	71	62
13	10	14	26	69	56
14	13	18	27	70	44
15	16	26	28	51	21
16	28	33.	29	20	5.6
17	12	15	30	4.8	1.2
18	10	14			

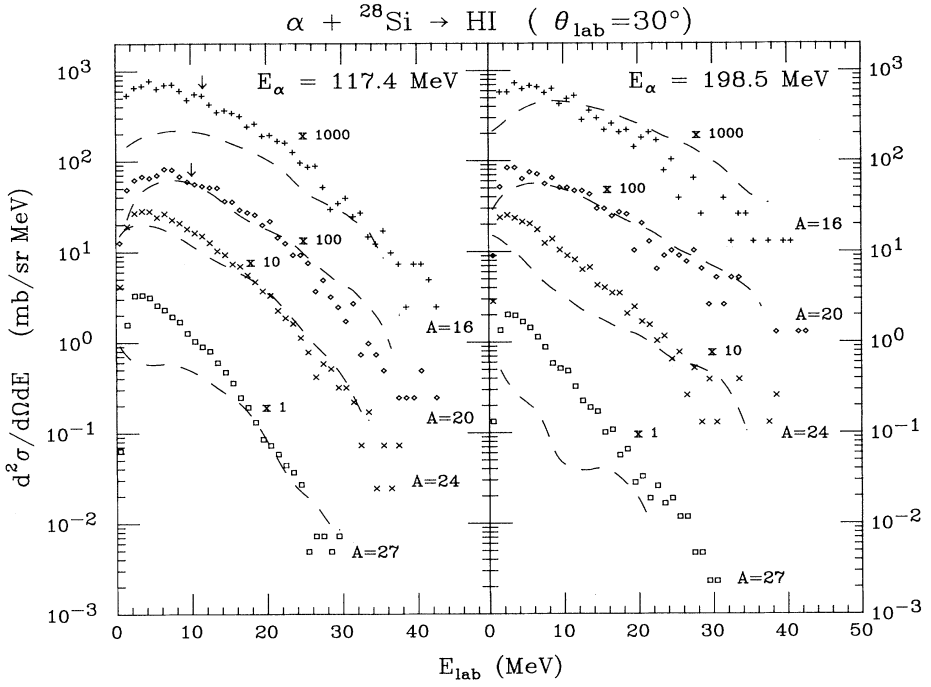

FIG. 2. Energy spectra observed at 30° for representative fragment mass values, as indicated on figure. Left figure is for bombardment at 117.4 MeV and right is for 198.5 MeV. Dashed lines are predictions of intranuclear cascade/statistical decay calculations [30]. Cross sections have been multiplied by factors shown on figure.

transverse recoil components. In regard to the question of multifragmentation, it is of interest to examine the backward-angle angular dependence of the data. For $\Theta > 90°$ the differential cross sections are nearly constant for $A = 7$ fragments. There is also an inversion of the dependence of the differential cross section on fragment mass; i.e., at forward angles the yields of the heavy fragments are enhanced, whereas at backward angles the reverse is true. In addition, the backward-angle cross sections are significantly larger at 198.5 MeV than at 117.4 MeV. This behavior is suggestive of a mechanism in which fragmentation of the highly-excited system into two or more

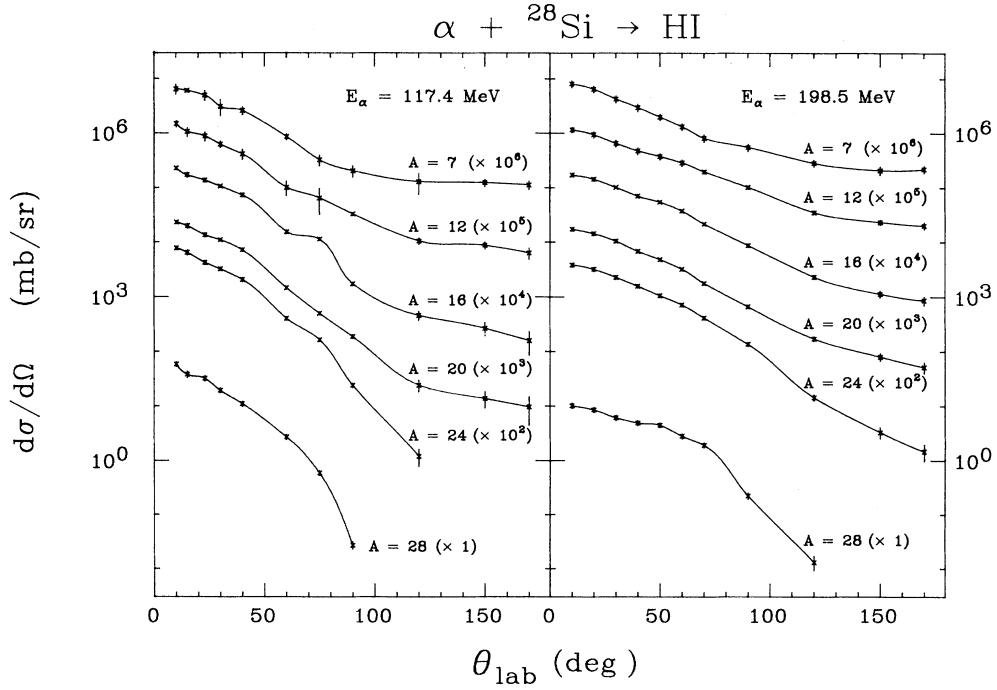

FIG. 3. Angular distributions for several representative mass values (as indicated on figures). Left figure is for bombardment at 117.4 MeV and right is for 198.5 MeV. The experimental data points are joined by solid lines to guide the eyes. Cross sections have been multiplied by factors shown on figure.

complex fragments may produce a large angular spreading of the products toward backward angles.

In Fig. 4 the angle- and energy-integrated mass distributions for the two energies are shown; these values are also given in Table I. Combined statistical plus systematic errors range from about 10% for light fragments to 20% for the heaviest fragments. Extrapolations of the energy spectra to zero energy and angular distributions to the beam axis are accounted for in the tabulated values and included in the error estimates. At both energies the yield patterns are quite similar. There is a clear shift toward enhanced population of lower masses for the higher excitation energy. The average mass loss relative to the composite nucleus (CN), $\langle \Delta A \rangle = A_{\rm CN} - A(\text{fragment})$, from these data is -9.8 nucleons at 117.4 MeV and -11.5 nucleons at 198.5 MeV. Intranuclear cascade calculations indicate that mass loss, ΔA, is correlated with excitation energy of the system; this result suggests that only a small fraction of the additional 80 MeV of projectile energy is translated into internal excitation energy in these collisions. Another significant feature of the mass distributions is the favored feeding of $A = 4n$ nuclei in the de-excitation of the primary fragments. The large mass losses ΔA, discussed above and relatively low momentum transfers (see below) found for this system can be reconciled by a picture in which emission of alpha particles – either sequential or simultaneous – provides the central pathway for de-excitation of the primary residues. This is also consistent with the previous discussion of the angular distributions.

The observed dependence of the fragment cross sections on ejectile mass in the ^{4}He + ^{28}Si system differs from that for intermediate-energy He-induced reactions on heavier targets [23,24]. For heavy targets one observes a significant contribution of intermediate-mass fragments ($6 \leq A \leq 30$), for which the cross sections follow a power-law decrease with increasing ejectile mass [25]. The opposite trend is observed in the present data (Fig. 4). This contrasting behavior implies that for the relatively diffuse ^{28}Si target, formation of complex fragments is less probable, either due to dynamical constraints associated with increased transparency (and therefore lower average excitation energy) or insufficient matter density in the hot intermediate system to permit coalescence of these fragments.

Total reaction cross sections for the two energies are listed in Table II. These values represent the direct sum of the $A \geq 6$ cross sections and do not account for either missing cross section due to possible total disintegration of the system into H and He, or double counting due to multifragment-emission processes. The results are in relatively good agreement with other data [13,14,26] and indicate the expected decrease in the reaction cross section with increasing energy due to target transparency. The results are compared with calculations of σ_R by Webber [27], Kox [28] and Karol [29] in Table II. The reported cross sections are significantly lower than the model calculations.

In Fig. 5, the average longitudinal linear momentum transfer for each isobar, $\langle p_{\|}(A) \rangle$ is plotted versus the observed fragment mass. Values of $p_{\|}$ were calculated from (1) the measured fragment velocity distributions, assuming the average fragment velocity is unchanged by statistical particle evaporation, and (2) the average mass of the fragment prior to decay was $\langle A \rangle = 29$ at 117.4 MeV and $\langle A \rangle = 28$ at 198.5 MeV. The choice of $\langle A \rangle$ was based upon the results of intranuclear cascade (CLUST) predictions [30] for these two systems. However, within the experimental errors the results are not strongly dependent on this assump-

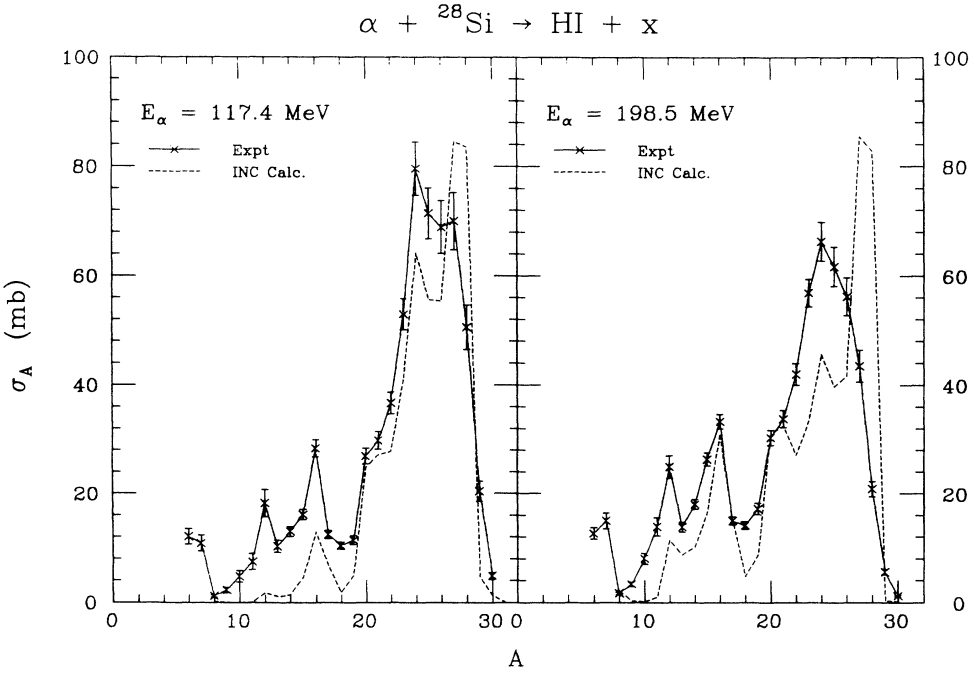

FIG. 4. Measured isobaric cross sections (solid line) for $A \geq 6$ fragments produced in 117.4 MeV (left) and 198.5 MeV (right) ^{4}He reactions with ^{28}Si. The dashed line is a prediction from an intranuclear cascade/statistical decay calculation [30].

TABLE II. Total Reaction Cross Sections (mb).

E_α	σ_R (exp)	σ_R (predicted)[a]	σ_R (predicted)[b]	σ_R (predicted)[c]
117.4 MeV	670	950	1212	1230
198.5 MeV	640	950	1133	1104

[a] Reference [27].
[b] Reference [28].
[c] Reference [29].

tion. For targetlike residues, the ratios of $\langle p_\parallel(A)\rangle/p_{\rm beam}$ fall well below unity, supporting the previous assumption that these fragments can only be produced in reactions which impart small linear momenta and excitation energy to the struck nucleus. As the fragment mass decreases, the increased violence of the collision is indicated by increasing linear momentum transfer, which approaches the fusion limit for the lightest complex fragments. Comparison of the 117.4 MeV results with those at 198.5 MeV demonstrates the expected decrease in $\langle p_\parallel(A)/p_{\rm beam}\rangle$ for the higher velocity projectile due to the linear momentum carried off by precompound emission processes. The cross-section-weighted value of the longitudinal linear momentum transfer, $\langle p_\parallel\rangle$ averaged over all masses, is 460 MeV/c at 117.4 MeV incident energy and 450 MeV/c at 198.5 MeV. This corresponds to fractions of the beam momentum, $\langle p_\parallel\rangle/p_{\rm beam}$, of 0.49 ± 0.04 at the lower energy and 0.37 ± 0.04 at the upper energy. These data make it possible to extend the target systematics of the linear momentum transfer to lighter nuclei, as shown in Fig. 6. Here previous results [15] for $\langle p_\parallel\rangle/p_{\rm beam}$ are compared with the present results as a function of target mass for E/A = 35 MeV ^{4}He ions. The value of 0.45 ± 0.04 interpolated from the present data is observed to follow the decrease indicated by Ref. [15]. From the systematics shown in Fig. 6, it is apparent that linear momentum transfer (and correspondingly, imparted excitation energy) decreases with decreasing target mass. This behavior is most simply understood in terms of the increasing ratio of the cross-sectional areas for the diffuse surface relative to the central matter density for decreasing target mass.

IV. DISCUSSION

A. Model calculations

Interpretation of these data requires a model that can account for both the collision dynamics and the statistical decay of the primary reaction products. In this section we compare the data with predictions of the intranuclear cascade code CLUST [30] to develop the reaction dynamics, and the DFF code [31] to account for statistical decay of the primary fragments. The CLUST code has been developed specifically for ^{1}H-, ^{2}H-, and ^{4}He-induced reactions below about 1 GeV incident energy. Comparison of CLUST with ISABEL [32], a generalized INC code for complex projectiles, shows that for the present sys-

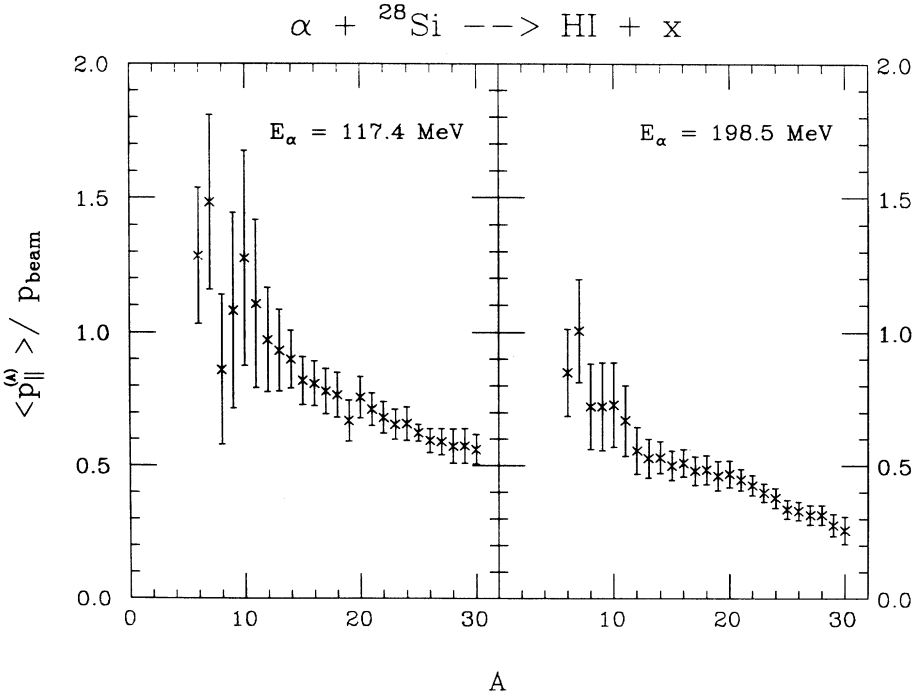

FIG. 5. Ratio of average linear momentum transfer parallel to the beam momentum as a function of observed ejectile mass.

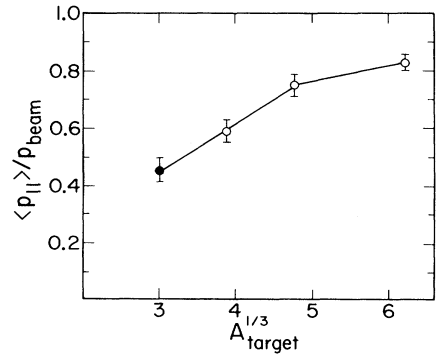

FIG. 6. Ratio of total average linear momentum transfer to the beam momentum as a function of target mass for $E/A = 35$ MeV ^{4}He-induced reactions. The solid point is derived from this work; open points are from Ref. [15].

tems the energy dissipation predicted by ISABEL is too low to account for these results. This underprediction is largely due to the dominance of quasifree scattering processes in the ISABEL dynamics. Similar calculations with the standard INC code have recently been performed for proton-induced reactions by Tang *et al.* [33].

As indicated in Fig. 1, the spectral shapes predicted by the CLUST code are in relatively good agreement with the data. The calculations predict somewhat flatter slopes for the spectra at forward angles and steeper slopes at backward angles for both energies. However, for angles in the range of 30° to 60°, which comprise a significant fraction of the cross section, the agreement with both absolute cross sections and spectral shapes is quite good. These same conclusions apply to all isobaric products (Fig. 2), except for deviations in the absolute cross sections for near-target and very light ($A \leq 16$) products. In general the agreement is better at 198.5 MeV than at 117.4 MeV.

Despite the relatively satisfactory fits to the fragment spectra, a significant disagreement appears when the angular distributions are compared with the model (Fig. 7). At forward angles the calculations fall well below the data whereas they seriously overpredict the yields of near-target products in the vicinity of the quasielastic recoil angle. This has been noted previously in the 180 MeV p + ^{27}Al reaction [14] and demonstrates a major failure of the standard intranuclear cascade model for light target nuclei in this energy regime; i.e., it overpredicts quasifree scattering mechanisms at the expense of more complex scatterings which lead to higher linear momentum transfers and deposition energies.

In Fig. 5 the isobaric yields at each energy are compared with the model. The downward shift in the experimental mass distributions relative to the calculation is apparent at both energies; this discrepancy is most noticeable in the region of the quasielastic products. In addition, the failure of the calculation to reproduce the yields of the lightest products ($A < 20$) is also apparent, although at 198.5 MeV there is significant improvement in this respect relative to the 117.4 MeV results. All of these comparisons indicate that the reaction dynamics incorporated in the intranuclear cascade calculation do not result in sufficiently large deposition energies in ^{4}He-induced reactions on light target nuclei. The calculation does succeed in qualitatively reproducing the enhanced yields for $A = 4n$ products.

B. Applications of data

As indicated in the introduction, an understanding of intermediate-energy light-ion interactions is important to studies of cosmic-ray related phenomena associated with space-radiation effects and nuclear astrophysics.

Cosmic-ray nuclei represent an important source of bit upset generation in microelectronic devices [18]. An essential ingredient for any attempt to account for these radiation-induced errors is the availability of reliable doubly differential cross-section information, $d^2\sigma/d\Omega\, dE$, for cosmic-ray-induced reactions in the material of interest: i.e., primarily silicon and oxygen. Of particular concern in evaluating radiation effects is the possibility that energetic heavy recoil fragments may enhance the magnitude of radiation effects due to their high ionization density, proportional to AZ^2 of the fragment. The large excess of energetic heavy fragments at forward angles (relative to theoretical predictions) observed in these studies (see Fig. 7), as well as for the p + ^{27}Al system [14], indicate that heavy recoils may be a significant contributor to error generation in silicon chips exposed to cosmic-ray fluxes.

Three problems of astrophysical interest are also addressed by these data. The first relates to the origin of galactic cosmic rays (GCR). Measurements [17] of the isotopic composition of galactic cosmic rays reveal a significant enrichment of neutron-excess Ne and Mg isotopes relative to their interstellar medium (ISM) ratios. This observation suggests that GCR progation may be associated with an r-process-like environment. However, in order to test such theories, it is essential to understand the modifications to the primary source flux due to nuclear reactions which occur during transport through the interstellar medium. Corrections for these processes depend on an accurate knowledge of cross sections for reactions between heavy cosmic-ray primaries (such as ^{28}Si) with hydrogen and helium (the dominant components of the interstellar medium).

In Table III isotopic ratios for the stable Ne and Mg isotopes are compared with the cross-section ratios for these data (Table I) and for the 180-MeV p + ^{27}Al reaction [14]. The data demonstrate that these spallation processes, mass numbers $A = 24$–26 (Mg isotopes on a cosmic-ray time scale, except for ^{26}Al) and $A = 20$–22 (Ne isotopes) are populated with roughly equal probability. Thus one would expect enrichment of neutron-excess species relative to solar system abundances in the spectrum of neon and magnesium isotopes formed in spallation of Si primaries in the cosmic-ray flux. Similarly, for mass numbers $A = 16$–18 (oxygen) enhanced production is observed for the neutron-excess isotopes; however, at this level contributions from spallation of ^{20}Ne and ^{24}Mg primaries also become important. Thus, the observation of enriched ratios for neutron excess isotopes in

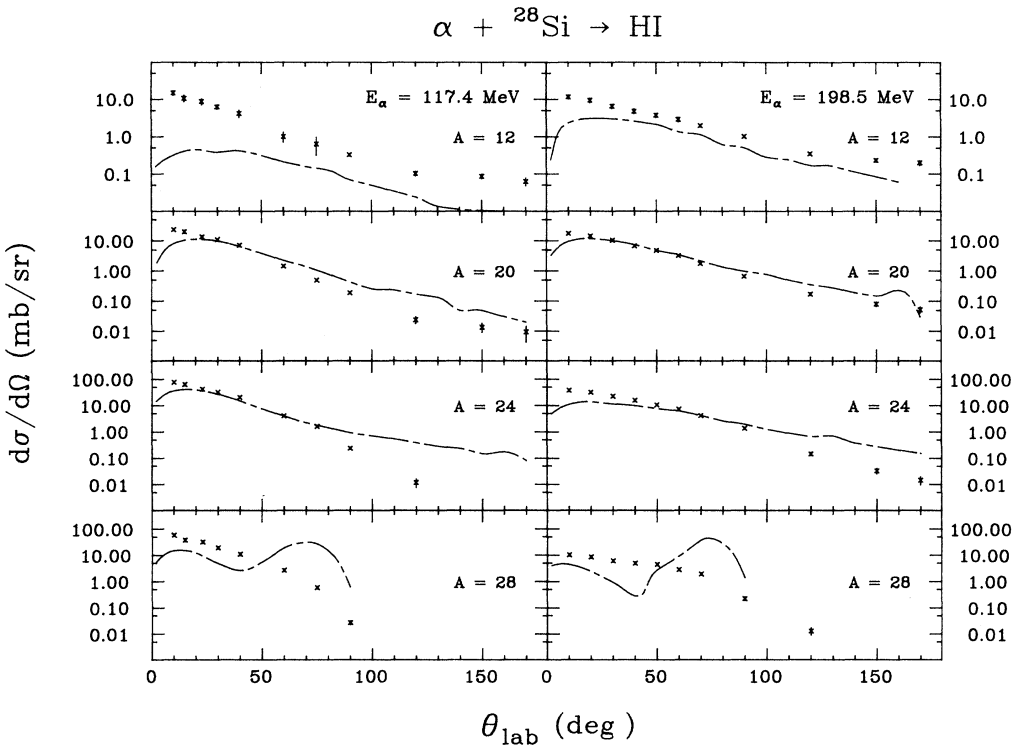

FIG. 7. Angular distributions for several representative mass values (as indicated on figures). Left figure is for bombardment at 117.4 MeV and right is for 198.5 MeV. Dashed lines are predictions of intranuclear cascade/statistical decay calculations [30]. Calculations do not predict any yield for $A = 7$. Cross sections have been multiplied by factors shown on figure.

the cosmic-ray flux relative to solar-system material is at least in part a consequence of spallation reactions experienced by any primary flux in passing through the interstellar medium [16, 34]. Quantative evidence for anomalies in the cosmic-ray isotopic composition can only be understood after correction for these spallative processes.

A second, similar application of these data relates to the abundances of secondary nuclei produced in meteorites by GCR-induced spallation reactions during the meteorite lifetime. These measured cross sections, in conjunction with isotope ratios observed for a given meteorite, can be used to infer information on its exposure geometry and the history of GCR fluxes [35].

A third astrophysical problem of related interest is the nucleosynthesis of the elements lithium, berylium, and boron(LiBeB). The abundances of the nuclides ^{6}Li, ^{9}Be, ^{10}B, and ^{11}B can be understood as primarily due to reactions of galactic-cosmic-ray H and He with He and CNO nuclei in the interstellar medium (CNO = carbon, nitrogen, and oxygen) [16]. One open question concerning this model is the possible contribution of heavier target species in the interstellar medium (e.g., Ne, Mg, and Si spallation) to the production of LiBeB. Since the relative abundances of these target-source elements are smaller than for CNO (C/N/O/Ne/Mg/Si = 0.61/0.13/1.00/0.14/0.06/0.06), the heavier species can only be important if the formation cross sections for LiBeB are significantly higher than for CNO. The cross-section results for LiBeB listed in Table I are slightly lower for Si than for CNO targets [36] at these energies. This suggests that the high energy cross sections for ^{20}Ne and ^{24}Mg, the other two major contributors to GCR synthesis of LiBeB, are comparable. Inclusion of these ^{4}He + ^{28}Si results and those of Ref. [14] into the GCR calculations of Walker *et al.* [16] serves to increase the absolute production rates of ^{6,7}Li, ^{7}Be, and ^{10,11}B by

TABLE III. Isotope number ratios of neon and magnesium isotopes in ISM and GCR [17] compared with cross section ratios for corresponding mass numbers in p + ^{27}Al reaction [14] and these data (Table I).

	^{20}Ne : ^{21}Ne : ^{22}Ne	^{24}Mg : ^{25}Mg : ^{26}Mg
ISM	1.0 : 0.024 : 0.073	1.0 : 0.13 : 0.14
GCR	1.0 : 0.25 : 0.67	1.0 : 0.28 : 0.30
180 MeV p + ^{27}Al	1.0 : 1.12 : 1.03	1.0 : 1.13 : 1.40
198.5 MeV ^{4}He + ^{28}Si	1.0 : 0.55 : 1.50	1.0 : 0.94 : 0.85

about 2–4 % and to have little effect on the isotope ratios. Thus, the contribution of species heavier than CNO to the LiBeB formation in galactic cosmic-ray interactions with the interstellar medium appears to be small and does not significantly perturb the existing scenario for LiBeB nucleosynthesis.

V. SUMMARY

The principal conclusion to be drawn from these studies of intermediate energy ^{4}He ions on light target nuclei is that excitation energy deposition and momentum transfer in the collision stage are significantly larger than predicted by intranuclear cascade/statistical decay predictions. Experimentally, this is supported by the strongly forward-peaked angular distributions and mass distributions which are skewed to lighter masses than predicted by the code. This discrepancy is best understood in terms of the relative importance of quasifree scattering events compared to multiple scatterings [14], as has been noted previously for intermediate-energy proton-induced reactions [14, 37].

These data suggest that the decay of the highly excited residues formed in these reactions is dominated by multibody ($n \geq 3$) processes, either sequential or instantaneous. In support of the multibody character of the deexcitation process, one observes that the yields of light fragments ($A \leq 16$) in the backward hemisphere are significantly enhanced at the higher energy and that the Coulomb peaks of these spectra are significantly lower than expected for a two-body breakup mechanism. In this respect (i.e., spectral shapes and backward-angle yields) the intranuclear cascade/statistical decay code describes the data satisfactorily, as might be expected since it incorporates sequential multibody emission in the deexcitation process.

These data also have relevance to radiation-damage studies in microelectronic devices exposed to intermediate energy light-charged particle fluxes. Most significant in this regard is the much larger probability of producing energetic complex fragments ($Z \geq 3$) relative to predictions of cascade models which are generally employed in radiation damage simulations. Due to the much larger specific ionization of such fragments, they may constitute a larger component of the total radiation damage than previously believed.

The data also impact on three problems of astrophysical interest. First, with regard to the question of lithium, beryllium and boron nucleosynthesis in galactic-cosmic-ray interactions with the interstellar medium, the measured cross sections are consistent with arguments [34] that nuclei heavier than oxygen contribute negligibly to the abundances of these elements. Of greater significance, these results emphasize the importance of transport corrections in attempts to infer the primary composition of galactic cosmic rays from observed isotope ratios. These cross-section data, along with those of Ref. [14], demonstrate that proton- and alpha-particle-induced spallation reactions during transport significantly enhance the yields of neutron-rich nuclides. Thus, the observation of neutron-rich species in the observed cosmic-ray yields [17] may be at least in part due to this effect.

ACKNOWLEDGMENTS

The authors wish to acknowledge the IBM Corporation for the primary support of this work and in particular H.C. Tang for many valuable conversations concerning the intranuclear cascade calculations. We also acknowledge support from the U.S. Department of Energy, and the National Science Foundation for partial support.

[1] *Proceedings of the Symposium Towards a Unified Picture of Nuclear Dynamics*, 1991, edited by Y. Abe, S.M. Lee, and F. Sakata, AIP Conf. Proc. No. 250 (AIP, New York, 1991); in *Proceedings of the Symposium on Formation and Decay of Hot Nuclear Matter*, Dallas, TX, 1989, edited by J.B. Natowitz (World Scientific, Singapore, 1989).
[2] J.R. Wu, C.C. Chang, and H.D. Holmgren, Phys. Rev. C **19**, 370 (1979); **19**, 659 (1979); **19**, 698 (1979).
[3] R. Stokstad, Comments Nucl. Part. Phys. **13**, 231 (1984).
[4] H.M. Blann, Phys. Rev. C **31**, 1245 (1985).
[5] H. Machner, Phys. Rep. **127**, 309 (1985); Z. Phys. A **321**, 577 (1985).
[6] W.G. Lynch, Annu. Rev. Nucl. Sci. **37**, 493 (1987).
[7] W.A. Friedman, Phys. Rev. C **42**, 667 (1990).
[8] J. Aichelin, A. Rosenhauer, G. Peilert, H. Stöcker, and W. Greiner, Phys. Rev. Lett. **58**, 1926 (1987).
[9] S.E. Koonin and J. Randrup, Nucl. Phys. **A474**, 183 (1987).
[10] J. Bondorf *et al.*, Nucl. Phys. **A443**, 1245 (1985).
[11] D.H.E. Gross and H. Massman, Nucl. Phys. **A471**, 339c (1987).
[12] A. Gökmen, H. Breuer, A.C. Mignerey, B.G. Glagola, K. Kwiatkowski, and V.E. Viola, Phys. Rev. C **29**, 1595 (1984).
[13] A. Gökmen, G.J. Mathews, and V.E. Viola, Phys. Rev. C **29**, 1606 (1984).
[14] K. Kwiatkowski, S.H. Zhou, T.E. Ward, V.E. Viola, H. Breuer, G.J. Mathews, A.C. Mignerey, and A. Gökmen, Phys. Rev. Lett. **50**, 1648 (1983).
[15] T. Batsch, J. Blanchot, Q. Chen, J. Croncon, M. Fatyga, A. Gizon, J. Jastrzebski, H. Karwowski, W. Kurcewicz, A. Lleres, T. Mroz, L. Pienkowski, P.P. Singh, S.E. Vigdor, and I. Zychor, Phys. Lett. B **189**, 287 (1987).
[16] T.P. Walker, G.J. Mathews, and V.E. Viola, Astrophys. J. **229**, 745 (1985).
[17] M.E. Weidenbeck and D.E. Greiner, Phys. Rev. Lett. **46**, 682 (1981).
[18] D.M. Ngo, J.W. Wilson, T.N. Fogarty, and W.W. Buck, IEEE Trans. Nucl. Sci., Vol NS-38, 2 (1991); see also IEEE Trans. Nucl. Sci., Vol NS-31, No. 6 (1984).
[19] G. Gabor, W. Schimmerling, D. Greiner, P. Lindstrom, and F. Beiser, Nucl. Instrum. Methods **130**, 65 (1975).
[20] K. Kwiatkowski, V.E. Viola, W.G. Wilson, S.H. Zhou,

and H. Breuer, Nucl. Instrum. Methods **225**, 65 (1984).
[21] B. Kolb, Lawrence Berkeley Laboratory Report LBL 16128, 1983; N.R. Yoder (unpublished).
[22] F. St-Laurent, M. Conjeaud, R. Dayras, S. Harar, H. Oeschler, and C. Volant, Nucl. Phys. **A422**, 307 (1984).
[23] L.G. Sobotka, M.L. Padgett, G.J. Wozniak, G. Guarino, A.J. Pacheco, L.G. Moretto, Y. Chan, R.G. Stokstad, I. Tserruya, and S. Wald, Phys. Rev. Lett. **51**, 2187 (1983).
[24] K. Kwiatkowski, J. Bashkin, H. Karwowski, M. Fatyga, and V.E. Viola, Phys. Lett. B **171**, 41 (1986).
[25] J. Zhang, S. Rose, K. Kwiatkowski, K. Stith, D. Bonser, L.W. Woo, and V.E. Viola, Indiana University Nucl. Chem. Report INC-40007-56 (1988).
[26] R.M. DeVries and J.C. Peng, Phys. Rev. C **22**, 1055 (1980); N.J. DiGiacomo and R.M. DeVries, Comments Nucl. Part. Phys. **12**, 111 (1984).
[27] W.R. Webber, J.C. Kish, and D.A. Schrier, Phys. Rev. C **41**, 520 (1990).
[28] S. Kox, A. Gamp, R. Cherkaoui, A.J. Cole, N. Longequeue, J. Menet, C. Perrin, and J. Viano, Nucl. Phys. **A420**, 162 (1984).
[29] P.J. Karol, Phys. Rev. C **11**, 1203 (1975).
[30] G.J. Mathews, B.G. Glagola, R.A. Moyle, and V.E. Viola, Phys. Rev. C **25**, 2181 (1982).
[31] I. Dostrovsky, Z. Fraenkel, and G. Friedlander, Phys. Rev. **116**, 683 (1959).
[32] Y. Yariv and Z. Frankel, Phys. Rev. C **20**, 2227 (1979); **26**, 460 (1982).
[33] H.H.K. Tang, G.R. Srinivasan, and N. Azziz, Phys. Rev. C **42**, 1598 (1990).
[34] S.M. Austin, Prog. Part. Nucl. Phys. **7**, 1 (1981).
[35] B. Zanda, G. Maline, and J. Audouze, Earth Planet Sci. Lett. **94**, 171 (1989).
[36] S.M. Read and V.E. Viola, At. Data Nucl. Data Tables **31**, 359 (1984).
[37] L.W. Woo, K. Kwiatkowski, and V.E. Viola, Phys. Lett. **132B**, 283 (1983).